Computational and Theoretical Chemistry 1099 (2017) 87–91

Contents lists available at ScienceDirect

Computational and Theoretical Chemistry

journal homepage: www.elsevier.com/locate/comptc

DFT evidence of unforeseen bending in linearly fused polycyclic rings of hexasilabenzenoids

Aayush D. Gupta, Jyotsna S. Arora *

Department of Chemical Engineering, Institute of Chemical Technology, Nathalal Parekh Marg, Matunga, Mumbai 19, India

ARTICLE INFO

Article history:
Received 19 September 2016
Received in revised form 7 November 2016
Accepted 7 November 2016
Available online 10 November 2016

Keywords:
Hexasilabenzene
Aromatic
B3LYP
Reorganizational energy
Optoelectronics

ABSTRACT

The electronic structure and properties of linearly fused polycyclic hexasilabenzenoids (LF-PCHSBs) (*an all silicon – analogue of polyaromatic hydrocarbons*) is studied using Density Functional Theoretical (DFT) calculations at B3LYP/6-31G(*d,p*) level. The structure of LF-PCHSBs display chair like puckering with the formation of ordered pair of ripples. On increasing the number of rings, the oligomers exhibits ~13° bending. The analysis of orbitals, reorganizational energy (*RE*) and electronic distribution properties demonstrated an aberrant behaviour with increasing length of PCHSB units. Lower the value of *RE* and uniform electronic distribution along with induced bending of the molecular system, more efficiently these oligomers exhibit the optoelectronics candidacy. The *RE* also helps to authorize the suitability of material for optoelectronic applications and thus assists in designing innovative molecules.

1. Introduction

Graphene and its silicon/germanium analogues have attracted attention of both experimental and theoretical chemists working all around the globe [1–9]. Recent studies on silicene; an *all Si – analogue of graphene*, have proposed its potential for future-generation high-speed, low power and nanochip-scale optoelectronic applications [5,6]. The high electrical conductivity and non-linear optical properties renders silicene as a favourable material for semiconductor optoelectronic devices. The above mentioned electrical properties of silicene are also exhibited by graphene [5,6]. However, unlike silicene, graphene does not possess a band gap. This property makes the use of graphene difficult concerning its application as a switch and in transistors [7–12].

Several theoretical researchers [1–14] have also predicted that the free-standing one atom thick silicene possesses a buckled structure, which is contrary to the observation in graphene. The linearly fused polycyclic rings of hexasilabenzenoids (LF-PCHSBs) can thus be considered to be a special case of silicene, as most of the chemical and physical properties are similar to it. The present case is similar to the polyaromatic hydrocarbon (PAH) oligomers that are used as model systems for studying the π-π interactions between graphene sheets [13].

The LF-PCHSBs are formed by fusion of multiple aromatic rings containing Si_nH_m ($n \neq m$) units. These PCHSBs can be visualized as small molecular traces of silicene where the terminal valency is being satisfied with hydrogen atoms. The X-ray diffraction (XRD) studies on the single crystal of hexasilabenzene (*monomer of silicene*) have confirmed various morphologies of Si_6H_6. The additional spectroscopic data confirms that Si_6H_6 crystallizes as a naphthalene solvate [1–4]. However, due to insufficient experimental data for the synthesis of silicene or LF-PCHSBs, it remains a quest to understand the fundamental aspects of this system. Theoretical computations may thus provide an in-depth view on the atomistic and electronic properties for these systems [15–20]. Li et al. [21] predicted that bucking & doping of silicene introduced several structural defects within the sheet.

The objective of the current study is to report the electronic and structural features of LF-PCHSBs, considering PCHSBs to be the prospective oligomers for formation of *Si* containing graphene-like sheets. The Density Functional Theoretical (DFT) studies of LF-PCHSB oligomers (n = 1–14) are performed to focus on the factors which affect the structural features of these molecules [22,23].

2. Computational methodology

All the DFT calculations were performed using Gaussian *09* program package [24] while Chemcraft 1.8 and GaussView 5.0 programs [25,26] were used for structure visualizations. The LF-PCHSB oligomers in the current study are the periodic structures with a constant *y* but varying *x*-axis (*viz.* constant *m* but an increasing *n* value) and the terminal valency is satisfied with H atoms.

* Corresponding author.
E-mail address: josharora@gmail.com (J.S. Arora).

http://dx.doi.org/10.1016/j.comptc.2016.11.010
2210-271X/

Initially, the most appropriate functional amongst B3LYP, PBE and B3PW91 was chosen by optimizing the simplest molecule; Si_6H_6 [1,2]. The 6-31G(*d*,*p*) basis set was used [1,2]. The absence of imaginary frequencies computed from the frequency calculations confirmed the structures are minima. The reported frequencies in the current study *viz.* for frequency of bending ($\upsilon_{bending}$) and frequency of puckering ($\upsilon_{puckering}$) are not contaminated by rotational and translational modes.

Natural bond orbital (NBO) analysis [27–32] as implemented in G*09* was performed to obtain the electronic distribution and the orbital energy gap of LF-PCHSBs. The rate of charge transport in electron rich LF-PCHSBs was evaluated using the reorganisation energy (*RE*). To calculate *RE*, structures of the oligomers were first optimized (denoted as *M*). Then single point energy (SPE) of the same molecule (*M*) but now deficient in one electron (denoted as M^+) was evaluated at the same level of calculation. This approach can be rationalised as $M^+//M$. The third and fourth steps of *RE* calculation are summarised as $M//M^+$. The corresponding energy difference between them is used to determine *RE* (Eq. (1))

$$RE = (E_2 - E_3) + (E_4 - E_1) \quad (1)$$

where E_1 is the electronic energy of the optimized structure (*M*), E_2 is the SPE of M^+, E_3 indicates the electronic energy obtained by optimizing the structure M^+ and E_4 is the SPE of M^+ with variation in charge and multiplicity as 0 and 1, respectively [33,34].

3. Results and discussion

3.1. Optimized structure and energetics

The optimized structures of Si_6H_6 with B3LYP, PBE and B3PW91 functionals are given in Fig. 1 and the comparison of the optimized parameters with the available experimental data is described in Table 1. The computed bond distances *viz.* r_{Si-Si} = 2.20–2.29 Å and r_{Si-H} = ~1.48 Å, evaluated using all the three functionals are in agreement with the earlier reports [1–4,35,36]. The experimentally determined dihedral angle for puckering in Si_6H_6 is ~33.7° [4]. However, it is observed that the computed data at B3LYP level matches well with the X-ray determined geometric parameters compared to the other two functionals. Further, the structure of Si_6H_6 obtained using B3LYP functional is more stable compared to those computed by B3PW91 and PBE functionals. Therefore, considering the trade-off between accuracy of the computed data along with computational speed, the B3LYP functional proves to be highly suitable for the current oligomeric system.

The B3LYP optimized structures and parameters of LF-PCHSBs with increasing number of rings (*n* = 1–14) in 1-D are given in the supporting information {ESI} (Fig. S1) and Table 2, respectively. For structures with rings from *n* = 1–8, the molecule is completely linear and flat, however, from *n* = 9–14, the monolayered chain exhibits significant bending at the centre. This bending of the molecule starting at *n* = 9 affects the symmetry of the entire molecule [19,20], thus modifying the point group (S) with an increase in chain length. In the current study, some of the symmetry elements within these molecules (*n* = 9–14) are lost, and hence these oligomers possess only a plane of symmetry with the point group 'C_s' (Table 2).

The stability of the molecules with increasing number of rings in 1-D is explained by binding energy atom^{-1} (ΔE) (Table 2) calculated by Eq. (2) [1,2]

$$\Delta E = E(Si_aH_b) - (a/2)E(Si_2H_2) + [(a-b)/2]E(H_2) \quad (2)$$

where '*a*' and '*b*' are number of Si and H atoms, respectively, and *E* is the electronic energy obtained from the optimized structure. The ΔE decreases with an increment in the number of rings (from −6.56 for Si_6H_6 (*n* = 1) to −65.42 eV for $Si_{58}H_{32}$ (*n* = 14)) indicating enhanced stability of LF-PCHSB oligomers. The Gibbs energy change of hydrogenation (ΔG) is further used to confirm the stability of the system and is calculated using Eq. (3) (Table 2).

$$\Delta G = G(Si_aH_b) - (a/2)G(Si_2H_2) + [(a-b)/2]G(H_2) \quad (3)$$

where '*a*' and '*b*' are number of Si and H atoms, respectively, and Gibbs energy is taken from the thermodynamic data of optimized structure. The negative values of ΔG in turn confirms the stability of the monolayered system with an increase in the 1-D length.

The electronic distribution within LF-PCHSBs was observed using the molecular electrostatic potential surface (MESP). The MESP diagrams of the selected molecules (*n* = 2, 4, 6 and 9) are given in ESI (Fig. S2). MESP elucidates the electrostatic potential onto the isoelectron density surface of the molecule and clearly explains the relative polarity within the molecule [37,38]. The high electron density regions are shown by red – yellow coloration while the blue region indicates positive ESP. In Fig. S2, there is an ordered distribution of electron cloud over all the rings and this confirms the efficient charge transfer scheme over the cloud [39,40]. As the length increases, the electrostatic potential scale

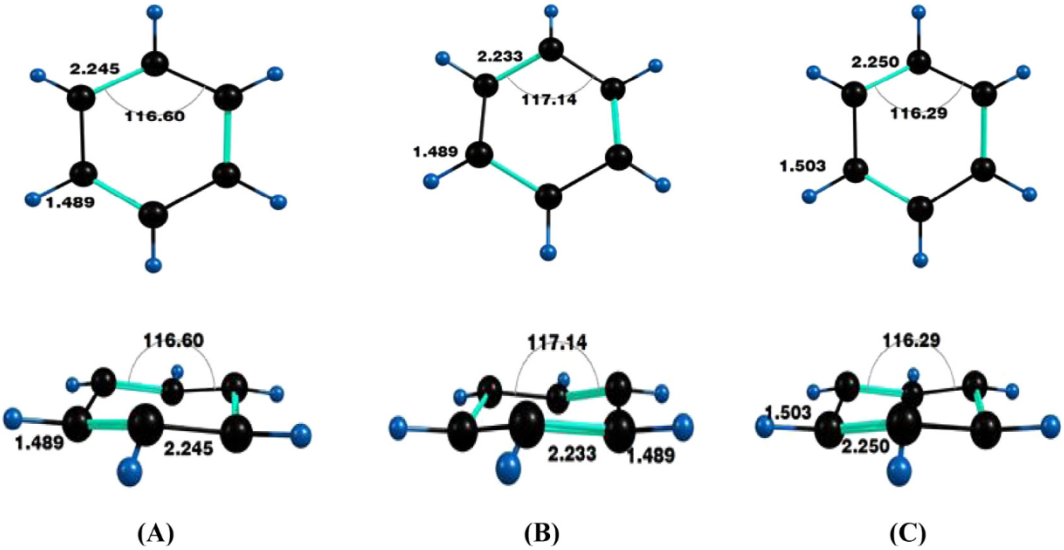

Fig. 1. DFT derived structures of Si_6H_6 (A) B3LYP (B) B3PW91 and (C) PBE level (distances in Å, bond angle in degree) (Top and Front view).

Table 1
Optimized parameters of Si_6H_6 with different functionals and comparison of the computed values with experimental data.

	B3LYP	B3PW91	PBE	Exp.[1–4,35,36]
[a]E_r, kcal mol^{-1}	0.00	181.98	621.23	–
r_{Si-Si}, Å	2.24	2.23	2.25	2.20–2.29[*]
r_{Si-H}, Å	1.49	1.49	1.50	1.48[**]
$\theta_{Si-Si-Si}$, degree	116.60	117.13	116.29	116[$]
Dihedral angle, degree	35.83	33.03	37.44	33.7[*]
E_{LUMO}, eV	−2.56	−2.62	−3.11	–
E_{HOMO}, eV	−5.74	−5.87	−5.31	–
E_g, eV	3.18	3.25	2.19	Non-zero

[a] E_r is the relative energy difference between the most stable structure of Si_6H_6 (obtained at B3LYP) and other two functionals.
[*] Jose and Datta [1,2,4] and Priyakumar et al. [3].
[**] Clabo and Schaefer [35].
[$] Nagase et al. [36].

Table 2
Optimized energy and puckering angle parameters of LF-PCHSB oligomers (n = 1–14).

n	MF	S	ΔE (eV)	ΔG (eV)	*IRE* (eV)	$\theta_{puckering}$, deg
1	Si_6H_6	D_{3d}	−6.56	−0.35	0.275	35.8
2	$Si_{10}H_8$	C_{2h}	−11.18	−0.59	0.157	35.67
3	$Si_{14}H_{10}$	C_{2h}	−15.74	−0.83	0.135	35.48
4	$Si_{18}H_{12}$	C_{2h}	−20.28	−1.06	0.122	35.54
5	$Si_{22}H_{14}$	C_{2h}	−24.80	−1.30	0.114	34.85
6	$Si_{26}H_{16}$	C_{2h}	−29.31	−1.54	0.107	34.79
7	$Si_{30}H_{18}$	C_{2h}	−33.83	−1.78	0.139	34.74
8	$Si_{34}H_{20}$	C_{2h}	−38.34	−2.02	0.096	34.7
9	$Si_{38}H_{22}$	C_s	−42.85	−2.25	0.203	34.70
10	$Si_{42}H_{24}$	C_s	−47.37	−2.49	0.146	34.69
11	$Si_{46}H_{26}$	C_s	−51.88	−2.73	0.132	34.7
12	$Si_{50}H_{28}$	C_s	−56.39	−2.97	0.121	34.68
13	$Si_{54}H_{30}$	C_s	−60.91	−3.20	0.112	34.7
14	$Si_{58}H_{32}$	C_s	−65.42	−3.44	0.103	34.7

also increases from −0.0132 to 0.0132 (n = 1) towards −0.0287 to 0.0287 (n = 14). This implies an increase in the electron density with an increase in n value.

The concept of *RE* is used to determine all the relevant charge transfer properties [41–44] in LF-PCHSBs. *RE* is classified into two types, internal and external which are denoted as *IRE* and *ERE*, respectively. *IRE* evaluates the energy of the system with an e^- added/removed from the molecule while *ERE* is the energy released during the morphological modifications in the structure. For the application of materials employed in the electronic devices [31–36], the *ERE* is not taken into consideration owing to the stiffness and rigidity of the material [41–44]. Hence, only *IRE* was computed in the current study. From n = 1 to 6, the *IRE* values decrease due to increase in the number of silicon atoms. The decreasing behaviour of *IRE* for LF-PCHSBs when bending starts indicates its application for optoelectronic materials (Table 2). As bending starts from n = 9 in LF-PCHSBs, the molecules possess lower *IRE* with extended charge separation and charge transport in the system but with an aberrant behaviour.

Due to bending within LF-PCHSBs, ripple formation is also observed. The uniformity or non-uniformity in the ripples depend upon the average puckering angle ($\theta_{puckering}$). The $\theta_{puckering}$ was calculated by averaging the dihedral angles in each ring and then taking an average on the whole molecule. This calculation was similar to that used for evaluating $\theta_{puckering}$ of benzene [41–44]. The $\theta_{puckering}$ remained almost constant for all the oligomers (n = 1–14) (Table 2) which signifies that bending does not distort the ordered ripples formed within the system.

3.2. Frequency analysis

The vibrational frequency analysis was performed in order to determine the frequencies of bending ($\upsilon_{bending}$) and puckering ($\upsilon_{puckering}$) in LF-PCHSBs. $\upsilon_{bending}$ is the lowest positive frequency given by the ground state optimized geometry of the oligomers. Higher value of $\upsilon_{bending}$ signifies large number of bending oscillations within the molecule, thus providing stability to the system. For LF-PCHSBs, $\upsilon_{bending}$ radically decreases from 104.11 cm^{-1} (n = 1) to 1.13 cm^{-1} (n = 8) (Table 3). Further decrease in $\upsilon_{bending}$ of LF-PCHSBs may generate negative or imaginary frequencies resulting in loss of molecular stability due to upward/downward vibrational forces. To overcome these forces, the higher PCHSB oli-

Table 3
The energy gap analysis of LF-PCHSBs.

n	MF	$-E_{HOMO}$, eV	$-E_{LUMO}$, eV	**E_g**, eV	n	MF	$-E_{HOMO}$, eV	$-E_{LUMO}$, eV	**E_g**, eV
1	Si_6H_6	5.740	2.560	3.180	8	$Si_{34}H_{20}$	4.681	4.010	0.671
2	$Si_{10}H_8$	5.324	3.085	2.239	9	$Si_{38}H_{22}$	4.654	4.055	0.599
3	$Si_{14}H_{10}$	5.086	3.415	1.671	10	$Si_{42}H_{24}$	4.634	4.090	0.543
4	$Si_{18}H_{12}$	4.938	3.629	1.309	11	$Si_{46}H_{26}$	4.601	4.119	0.482
5	$Si_{22}H_{14}$	4.838	3.774	1.064	12	$Si_{50}H_{28}$	4.605	4.142	0.463
6	$Si_{26}H_{16}$	4.769	3.877	0.892	13	$Si_{54}H_{30}$	4.595	4.162	0.433
7	$Si_{30}H_{18}$	4.718	3.953	0.766	14	$Si_{58}H_{32}$	4.587	4.178	0.409

*MF = Molecular Formula.

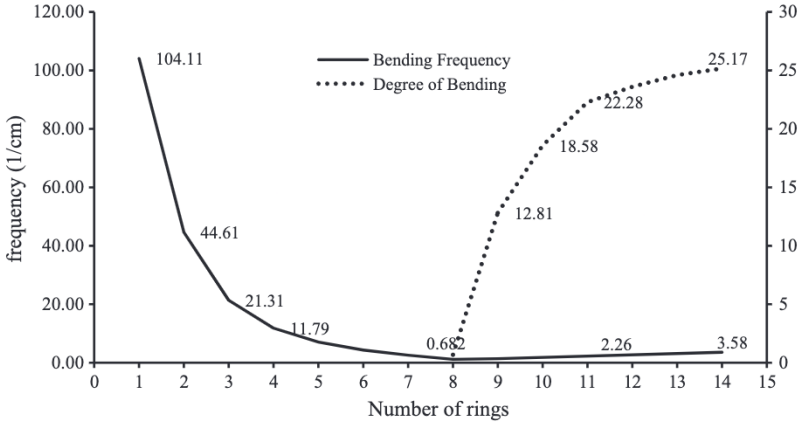

Fig. 2. Variation of bending frequency and degree of bending with ring increment in the monolayer.

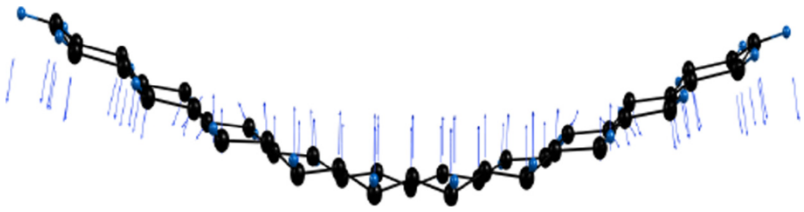

Fig. 3. System of ten rings vibrating at the lowest frequency (bending frequency).

gomers (n = 9–14) bend further, thus displaying an increase in the frequency values (1.38–3.17 cm^{-1}) from n = 9 to 14 (Table 3) [1–17].

$\upsilon_{puckering}$ refers to the vibrational frequency at which the whole molecule becomes puckered. Higher the puckering symmetry within the structure, greater is the tendency of each ring to exhibit uniform ripples across the surface [1–4]. In the current study, $\upsilon_{puckering}$ increases from 144.86 to 164.27 cm^{-1} (n = 1–8) rapidly. However, due to bending in n = 9 and 10 oligomers, there is only a marginal increase in $\upsilon_{puckering}$. This slow increment of $\upsilon_{puckering}$ after the start of bending (164.68 cm^{-1} (n = 9) to 166.79 cm^{-1} (n = 14)) implies stability of the bent system due to higher formation of ordered pair of ripples as the length of LF-PCHSBs increase (Fig. 2). Hence these vibrations ($\upsilon_{bending}$ and $\upsilon_{puckering}$) which result in maximized ordered ripple formation and symmetric bending in LF-PCHSBs confirms the stability of the system in spite of bending within the molecule.

3.3. Orbital analysis

The orbital energy gap ($\mathbf{E_g}$) values of LF-PCHSB oligomers are given in Table 3 while their HOMO-LUMO diagrams are given in ESI (Fig. S3). It is observed that $\mathbf{E_g}$ decreases from 3.180 eV in Si_6H_6 (n = 1) to 0.41 eV in $Si_{58}H_{32}$ (n = 14) (Table 3) which explains the stability of the molecular system as number of rings increase. From the HOMO-LUMO diagrams it is observed that as the value of n increases (for $n \geqslant 9$) bending starts, the orbitals start concentrating on the central part of the molecule. This is because negative vectors of bending forces are acting on the end atoms while positive vector forces acting within the central part of the molecule. Jensen discussed that the shapes of HOMO and LUMO resemble the trend of total electron density variation [45]. Thus in the current study, the concentration of orbitals (HOMO and LUMO) on the central part of the molecule can quantify that maximum electron density is cramped on the non-terminal rings of the higher oligomers ($n \geqslant 9$).

Fig. 3 shows the vibrational forces acting on the system of ten rings generated with high displacement amplitude which results in the vibrations of the molecule. The vibrational forces acting in the centre of the molecule are opposite to the direction of the forces acting on the terminal atoms. The bending in LF-PCHSBs from n = 9 units can be seen as the special case of '*ordered puckering effect*', thus providing enhanced stability to PCHSBs. Hence, it can be concluded that the absence of orbitals on the terminal atoms of the molecule allows it to vibrate freely, resulting in more bending and lower *IRE* values.

4. Conclusions

The structural and physical properties of LF-PCHSBs were thoroughly investigated. The *IRE* predicts the unexceptional behaviour due to bending. The vibrational frequency analysis reveals the formation of ripples and explains bending of the molecule. There is a significant change in the HOMO-LUMO energy differences with an increase in the number of rings ($n \leqslant 6$). For oligomers where $n > 6$, the $\mathbf{E_g}$ values change marginally even though the molecules exhibit significant bending. This decreasing trend in $\mathbf{E_g}$ with an increase in number of silicon atoms renders these molecules as highly efficient materials to be used in transistors and information processing along with other applications in optoelectronics.

Acknowledgement

This research did not receive any specific grant from funding agencies in the public, commercial, or not-for-profit sectors.

Appendix A. Supplementary material

Supplementary data associated with this article can be found, in the online version, at http://dx.doi.org/10.1016/j.comptc.2016.11.010. These data include MOL files and InChiKeys of the most important compounds described in this article.

References

[1] D. Jose, A. Datta, Structures and chemical properties of silicene: unlike graphene, Acc. Chem. Res. 47 (2014) 593–602.
[2] D. Jose, A. Datta, Understanding of the buckling distortions in silicene, J. Phys. Chem. C 116 (2012) 24639–24648.
[3] U.D. Priyakumar, T.C. Dinadayalane, G.N. Sastry, A computational study of the valence isomers of benzene and their group V hetero analogs, New J. Chem. 26 (2002) 347–353.
[4] D. Jose, A. Datta, Structures and electronic properties of silicene clusters: a promising material for FET and hydrogen storage, Phys. Chem. Chem. Phys. 13 (2011) 7304–7311.
[5] A. Kara, H. Enriquez, A.P. Seitsonen, L.C. Lew Yan Voon, S. Vizzini, B. Aufray, H. Oughaddou, A review on silicene – new candidate for electronics, Surf. Sci. Rep. 67 (2012) 1–18.
[6] P. Vogt, P. De Padova, C. Quaresima, J. Avila, E. Frantzeskakis, M.C. Asensio, A. Resta, B. Ealet, G. Le Lay, Silicene: compelling experimental evidence for graphene like two-dimensional silicon, Phys. Rev. Lett. 108 (2012) 155501–155505.
[7] C. Kamal, C. Aparna, B. Arup, S.K. Deb, Silicene beyond mono-layers-different stacking configurations and their properties, J. Phys.: Condens. Matter 25 (2013) 085508.
[8] Y. Wang, Y. Ding, Strain-induced self-doping in silicene and germanene from first-principles, Solid State Commun. 155 (2013) 6–11.
[9] M. Hu, Y. Shu, L. Cui, B. Xu, D. Yu, J. He, Theoretical two-atom thick semiconducting carbon sheet, Phys. Chem. Chem. Phys. 16 (2014) 18118–18123.
[10] P. Xu, Z. Yu, C. Yang, P. Lu, Y. Liu, H. Ye, T. Gao, Comparative study on the nonlinear properties of bilayer graphene and silicene under tension, Superlattices Microstruct. 75 (2014) 647–656.
[11] R.E. Roman, S.W. Cranford, Mechanical properties of silicene, Comput. Mater. Sci. 82 (2014) 50–55.
[12] L. Chen, H. Li, B. Feng, Z. Ding, J. Qiu, P. Cheng, K. Wu, S. Meng, Spontaneous symmetry breaking and dynamic phase transition in monolayer silicene, Phys. Rev. Lett. 110 (2013) 085504.
[13] S. Chakarova-Käck, A. Vojvodic, J. Kleis, P. Hyldgaard, E. Schröder, Binding of polycyclic aromatic hydrocarbons and graphene dimers in density functional theory, New J. Phys. 12 (2010) 013017.
[14] K. Ito, T. Hashizume, N. Ishii, T. Aida, Science 304 (2004) 1481.
[15] L. Tao, E. Cinquanta, D. Chiappe, C. Grazianetti, M. Fanciulli, M. Dubey, A. Molle, D. Akinwande, Silicene field-effect transistors operating at room temperature, Nat. Nanotechnol. 10 (2015) 227–231.
[16] K.K. Baldridge, O. Uzan, J.M.L. Martin, The silabenzenes: structure, properties, and aromaticity, Organometallics 19 (2000) 1477–1487.
[17] H. Liu, J. Gao, J. Zhao, Silicene on substrates: a way to preserve or tune its electronic properties, J. Phys. Chem. C 117 (2013) 10353–10359.
[18] N. Gao, J.C. Li, Q. Jiang, Tunable band gaps in silicene-MoS_2 heterobilayers, Phys. Chem. Chem. Phys. 16 (2014) 11673–11678.
[19] H. Vach, Electron-deficiency aromaticity in silicon nanoclusters, J. Chem. Theory Comput. 8 (2012) 2088–2094.
[20] Y.C. Cheng, Z.Y. Zhu, U. Schwingenschlögl, Doped silicene: evidence of a wide stability range, EPL 95 (2011) 17005.
[21] X. Li, J.T. Mullen, Z. Jin, K.M. Borysenko, M. Buongiorno Nardelli, K.W. Kim, Intrinsic electrical transport properties of monolayer silicene and MoS_2 from first principles, Phys. Rev. B. 87 (2013) 115418–115448.
[22] S. Li, Y. Wu, Y. Tu, Y. Wang, T. Jiang, W. Liu, Y. Zhao, Defects in silicene: vacancy clusters, extended line defects, and di-adatoms, Sci. Rep. 5 (2015) 1–7.
[23] Z.L. Liu, M.X. Wang, J.P. Xu, J.F. Ge, G. Le Lay, P. Vogt, D. Qian, C.L. Gao, C. Liu, J.F. Jia, Various atomic structures of monolayer silicene fabricated on Ag (1 1 1), New J. Phys. 16 (2014) 75006–75014.
[24] M.J. Frisch, G.W. Trucks, H.B. Schlegel, G.E. Scuseria, M.A. Robb, J.R. Cheeseman, G. Scalmani, V. Barone, B. Mennucci, G.A. Petersson, H. Nakatsuji, M. Caricato, X. Li, H.P. Hratchian, A.F. Izmaylov, J. Bloino, G. Zheng, J.L. Sonnenberg, M. Hada, M. Ehara, K. Toyota, R. Fukuda, J. Hasegawa, M. Ishida, T. Nakajima, Y. Honda, O. Kitao, H. Nakai, T. Vreven, J.A. Montgomery Jr., J.E. Peralta, F. Ogliaro, M.J. Bearpark, J. Heyd, E.N. Brothers, K.N. Kudin, V.N. Staroverov, R. Kobayashi, J. Normand, K. Raghavachari, A.P. Rendell, J.C. Burant, S.S. Iyengar, J. Tomasi, M. Cossi, N. Rega, N.J. Millam, M. Klene, J.E. Knox, J.B. Cross, V. Bakken, C. Adamo, J. Jaramillo, R. Gomperts, R.E. Stratmann, O. Yazyev, A.J. Austin, R. Cammi, C. Pomelli, J.W. Ochterski, R.L. Martin, K. Morokuma, V.G. Zakrzewski, G.A. Voth, P. Salvador, J.J. Dannenberg, S. Dapprich, A.D. Daniels, Ö. Farkas, J.B. Foresman, J.V. Ortiz, J. Cioslowski, D.J. Fox, Gaussian 09, in, Gaussian, Inc., Wallingford, CT, USA, 2009.
[25] R. Dennington, T. Keith, J. Millam, K. Eppinnett, W.L. Hovell, R. Gilliland, GaussView, Semichem Inc., Shawnee Mission, KS, 2009.
[26] G. Zhurko, D. Zhurko, ChemCraft, version 1.6, in: Build, 2009.
[27] E.D. Glendening, A.E. Reed, J.E. Carpenter, F. Weinhold, NBO Version 3.1., 1998.
[28] J. Foster, F. Weinhold, Natural hybrid orbitals, J. Am. Chem. Soc. 102 (1980) 7211–7218.
[29] A.E. Reed, F. Weinhold, Natural bond orbital analysis of near-Hartree–Fock water dimer, J. Chem. Phys. 78 (1983) 4066–4073.
[30] A.E. Reed, R.B. Weinstock, F. Weinhold, Natural population analysis, J. Chem. Phys. 83 (1985) 735–746.
[31] J.E. Carpenter, F. Weinhold, Analysis of the geometry of the hydroxymethyl radical by the "different hybrids for different spins" natural bond orbital procedure, J. Mol. Struct. (Theochem) 169 (1988) 41–62.
[32] A.E. Reed, L.A. Curtiss, F. Weinhold, Intermolecular interactions from a natural bond orbital, donor-acceptor viewpoint, Chem. Rev. 88 (1988) 899–926.
[33] M. Malagoli, J.L. Bredas, Density functional theory study of the geometric structure and energetics of triphenylamine-based hole-transporting molecules, Chem. Phys. Lett. 327 (2000) 13–17.
[34] Verahill, Approach to Computing Reorganizational Energies using NWCHEM, Australia, 2012. <http://verahill.blogspot.in/search/label/> (accessed 05.05.12).
[35] D.A. Clabo, H.F. Schaefer, The silicon analog of benzene–hexasilabenzene (Si_6H_6), J. Chem. Phys. 84 (1986) 1664–1669.
[36] S. Nagase, H. Teramae, T. Kudo, Hexasilabenzene (Si6H6). Is the benzene-like D6h structure stable?, J Chem. Phys. 86 (1987) 4513–4517.
[37] R.S. Madyal, J.S. Arora, DFT studies for the evaluation of amine functionalized polystyrene adsorbents for selective adsorption of carbon dioxide, RSC Adv. 4 (2014) 20323–20333.
[38] P. Wu, P. Du, H. Zhang, C. Cai, Microscopic effects of the bonding configuration of nitrogen-doped graphene on its reactivity toward hydrogen peroxide reduction reaction, Phys. Chem. Chem. Phys. 15 (2013) 6920–6928.
[39] W. Senevirathna, C.M. Daddario, G. Sauvé, Density functional theory study predicts low reorganization energies for azadipyrromethene-based metal complexes, J. Phys. Chem. Lett. 5 (2014) 935–941.
[40] G.R. Hutchison, M.A. Ratner, T.J. Marks, Hopping transport in conductive heterocyclic oligomers: reorganization energies and substituent effects, J. Am. Chem. Soc. 127 (2005) 2339–2350.
[41] R. Qin, W. Zhu, Y. Zhang, X. Deng, Uniaxial strain-induced mechanical and electronic property modulation of silicene, Nanoscale Res. Lett. 9 (2014) 521–527.
[42] S. Régis, H. Marie-Christine, S. Philippe, Spatial analysis of interactions at the silicene/Ag interface: first principles study, J. Phys.: Condens. Matter 27 (2015) 015002–15007.
[43] A.D. Hill, P.J. Reilly, Puckering coordinates of monocyclic rings by triangular decomposition, J. Chem. Inf. Model. 47 (2007) 1031–1035.
[44] Z. Tu, X. Huang, Y. Yi, Ambipolar charge-transport properties in 4,10-dihalogenated anthanthrone crystals: a theoretical study, J. Mater. Chem. C 3 (2015) 1913–1921.
[45] F. Jensen, Introduction to Computational Chemistry, second ed., John Wiley & Sons, England, 2013.